Interactions of divalent cations with calcium binding sites of BK channels reveal independent motions within the gating ring

Pablo Miranda[a,1], Teresa Giraldez[b], and Miguel Holmgren[a]

[a]National Institute of Neurological Disorders and Stroke, National Institutes of Health, Bethesda, MD 20892; and [b]Departamento de Ciencias Médicas Básicas, Instituto de Tecnologías Biomédicas y Centro de Investigaciones Biomédicas de Canarias, Universidad de La Laguna, 38071 La Laguna, Spain

Edited by Richard W. Aldrich, The University of Texas at Austin, Austin, TX, and approved November 3, 2016 (received for review July 12, 2016)

Large-conductance voltage- and calcium-activated K^+ (BK) channels are key physiological players in muscle, nerve, and endocrine function by integrating intracellular Ca^{2+} and membrane voltage signals. The open probability of BK channels is regulated by the intracellular concentration of divalent cations sensed by a large structure in the BK channel called the "gating ring," which is formed by four tandems of regulator of conductance for K^+ (RCK1 and RCK2) domains. In contrast to Ca^{2+} that binds to both RCK domains, Mg^{2+}, Cd^{2+}, or Ba^{2+} interact preferentially with either one or the other. Interaction of cations with their binding sites causes molecular rearrangements of the gating ring, but how these motions occur remains elusive. We have assessed the separate contributions of each RCK domain to the cation-induced gating-ring structural rearrangements, using patch-clamp fluorometry. Here we show that Mg^{2+} and Ba^{2+} selectively induce structural movement of the RCK2 domain, whereas Cd^{2+} causes motions of RCK1, in all cases substantially smaller than those elicited by Ca^{2+}. By combining divalent species interacting with unique sites, we demonstrate that RCK1 and RCK2 domains move independently when their specific binding sites are occupied. Moreover, binding of chemically distinct cations to both RCK domains is additive, emulating the effect of fully occupied Ca^{2+} binding sites.

SLO1 channel | FRET | allosteric regulation | divalent ions

The open probability of large conductance voltage- and Ca^{2+}-activated K^+ (BK) channels is allosterically tuned by two stimuli: transmembrane voltage and concentration of intracellular divalent cations (1–6). This intrinsic property makes them essential players in vital physiological processes where intracellular Ca^{2+} signaling is coupled to control of membrane voltage, such as neurotransmission or muscle function (7–10). Functional BK channels form tetramers of α-subunits (11, 12), each containing seven transmembrane helixes (S0–S6) and a large intracellular C-terminus region (13, 14). Even though BK channels can assemble with auxiliary subunits (13, 15–18), the α-subunit contains the sensors for voltage and divalent ions (4, 19). The voltage across the membrane is sensed by charged amino acids in transmembrane segments S2, S3, and S4 (20–24). Physiologically, BK channels can be modulated by intracellular Ca^{2+} and Mg^{2+}, which are sensed by the large C-terminus end of the α-subunit. This region folds into a pseudodimer of two regulator of conductance of K^+ domains (RCK1 and RCK2). Crystal structures of isolated BK channel C termini revealed that the tetramers of RCK dimers form a large structure called the "gating ring" (25–27). Each RCK domain contains one high-affinity Ca^{2+} binding site (Fig. 1 *A* and *B*, red circles) (2). The first site identified, named the Ca^{2+} bowl (28–30), is contained within the RCK2 domain (mainly D895 and D897 in the human BK channels), whereas another site was described in the RCK1 domain (including residues D362, D367, and E535) (2, 4, 31). Additionally, Mg^{2+} ions bind specifically, but with low affinity, to a site formed by four amino acids: two from the transmembrane region (D99 and N172) and two located in the RCK1 (E374 and E399) (Fig. 1*C*) (4, 32, 33). Increased intracellular concentration of both Ca^{2+} and Mg^{2+} shift the voltage dependence of activation toward more negative potentials, yet their mechanisms might be quite different (4, 32–41). In fact, Mg^{2+} is thought to interact directly with the RCK1 domain and the voltage sensor of the channel (32, 33).

Ca^{2+} binding sites in the gating ring are not equivalent. In addition to different affinities for Ca^{2+}, the structural and functional differences have been revealed by differential interactions with other divalent ions that can modulate BK channel activity. Thus, it has been established that Cd^{2+} selectively interacts with the RCK1 binding site, whereas Ba^{2+} acts exclusively through the Ca^{2+} bowl (2, 4, 32, 33, 42, 43). This property provides a unique opportunity to assess the independent role of each high-affinity binding site in the conformational rearrangements of the gating ring associated with BK channel function. Using patch-clamp fluorometry (44), we have previously detected changes in FRET triggered by Ca^{2+} binding to both high-affinity Ca^{2+} binding sites, consistent with large Ca^{2+}- and voltage-dependent structural rearrangements of the gating ring (45). Here we report motions of the gating ring that are triggered by the specific activation of single high-affinity binding sites by Mg^{2+}, Cd^{2+}, or Ba^{2+}. Consistent with previous functional studies (2, 43), we now show that Cd^{2+} induces structural rearrangements of the gating ring mediated by the RCK1 site, whereas Ba^{2+} induces motions through the Ca^{2+} bowl in the RCK2 domain. Interestingly, even though Mg^{2+} activates BK channels at its own binding site in the interface between the RCK1 and the voltage sensor domains (VSD) (Fig. 1*C*), our results indicate that this cation also binds to the Ca^{2+} bowl, inducing conformational changes in the gating ring. In all cases, activation of a

Significance

Large-conductance voltage- and calcium-activated K^+ (BK) channels are allosterically regulated by intracellular Ca^{2+} and voltage. The Ca^{2+} sensor is a large tetrameric structure called the "gating ring." Each subunit of this structure contains two distinct regulator of conductance of potassium (RCK) domains, each contributing one Ca^{2+} binding site. Both sites have a different selectivity for Ca^{2+}, Mg^{2+}, Cd^{2+}, and Ba^{2+}. Using FRET, we monitored the conformational changes of different regions of the gating ring upon binding of divalent ions. Our results reveal the existence of additive and independent motions by the two RCK domains that form the gating ring. These results indicate that the gating ring is a flexible structure capable of complex conformational changes that can be triggered specifically by different divalent ions.

Author contributions: P.M., T.G., and M.H. designed research; P.M. performed research; P.M., T.G., and M.H. analyzed data; and P.M., T.G., and M.H. wrote the paper.

The authors declare no conflict of interest.

This article is a PNAS Direct Submission.

Freely available online through the PNAS open access option.

[1]To whom correspondence should be addressed. Email: pablo.mirandafernandez2@nih.gov.

This article contains supporting information online at www.pnas.org/lookup/suppl/doi:10.1073/pnas.1611415113/-/DCSupplemental.

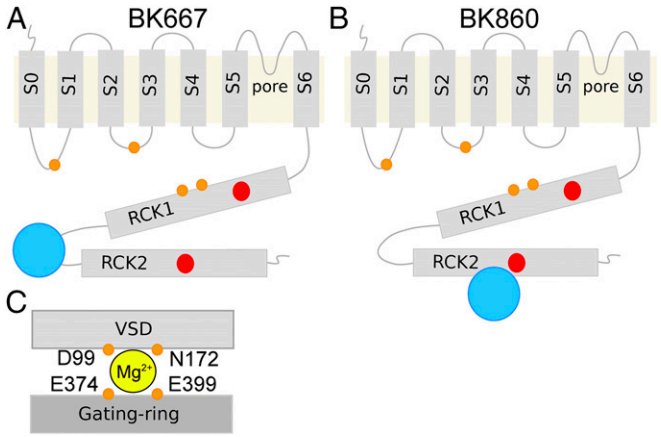

Fig. 1. Topological representations of the BK α-subunit. Blue circles represent fluorescent proteins in position 667 (*A*) or 860 (*B*). The transmembrane region includes the VSD (S1–S4), the pore domain (S5–S6), and an additional transmembrane helix (S0) that leads the N terminus to the extracellular side. The large cytoplasmatic region contains two RCK domains (RCK1 and RCK2). The high-affinity Ca^{2+} binding site of the RCK1 domain and the Ca^{2+} bowl at the RCK2 domain are represented with red circles. The four amino acids that form the Mg^{2+} binding site are represented by four orange circles at the approximate locations. (*C*) Schematic representation of the canonical Mg^{2+} binding site. Amino acids D99 and N172 from the VSD and E374 and E399 from the RCK1 domain coordinate Mg^{2+} (yellow circle).

single high-affinity binding site evoked significantly smaller FRET changes than those observed with Ca^{2+}. Taking advantage of the differential selectivity of the binding sites, we combined two species of divalent cations to show that both RCK domains can move independently. The addition of the effect by coincident activation of RCK1 and RCK2 emulates the effect of Ca^{2+}.

Results

Gating-Ring Rearrangements Elicited by Mg^{2+}. We previously described that insertion of fluorescent proteins at position 667 of BK α-subunit (Fig. 1*A*), located in the linker between RCK1 and RCK2, did not alter the function of the channel allowing the detection of voltage- and Ca^{2+}-dependent rearrangements of the gating ring (45). Fig. 2*A* shows conductance–voltage (G–V) curves for the BK667CY tetramers at voltage values from 0 to +260 mV with different Mg^{2+} concentrations. Similar to previous reports (32, 33, 35, 36, 39, 46, 47), when Mg^{2+} was increased from 0 to 100 mM the half-activation potential ($V_{1/2}$) shifted leftward from 176.5 ± 2.3 to 82 ± 1.4 mV. Fluorescent data acquired simultaneously in the same membrane patches are shown in Fig. 2*B*. In Mg^{2+}-free solutions, FRET between CFP and YFP occurred with low efficiency (*E*), rendering a value of 0.037 ± 0.004 (n = 14) at all voltages studied. This absence of detectable FRET signal suggests that in the absence of Mg^{2+} the fluorophores at position 667 in the tetramer are separated by at least 100 Å ($2R_0$). As the concentration of Mg^{2+} is increased, *E* augmented to an asymptotic value of 0.26 ± 0.004 (n = 14). These results show that the average distance between fluorophores is smaller as the gating ring rearranges in response to Mg^{2+} binding. Interestingly, the steep voltage dependence of *E* previously observed with Ca^{2+} in the 667 construct (45) is not as obvious when Mg^{2+} binds. In addition, the magnitude of the changes in *E* elicited by Mg^{2+} is about half of that induced by Ca^{2+} (45). The Mg^{2+}-dependent rearrangements of the gating ring follow sigmoidal relationships with apparent affinities (K_d) between 0.4 and 0.6 mM depending on the voltage (Fig. S1*A*).

How are Mg^{2+}-dependent rearrangements mediated? BK activation by Mg^{2+} has been functionally attributed to a site located at the interface between the gating ring's RCK1 domain and the VSD in the transmembrane region (Fig. 1*C*) (4, 32, 33). Mg^{2+} is coordinated by amino acids D99 and N172 from the VSD, and E374 and E399 from the RCK1 domain (4, 21, 32, 33, 37). It is thought that electrostatic interactions between bound Mg^{2+} and the voltage sensor are responsible for the coupling between the VSD and the opening of the gate (32), leading to a shift in the voltage dependence of the channel. To test whether the movements of the gating ring detected in response to Mg^{2+} are mediated by this canonical Mg^{2+} binding site, we introduced the mutation D99A (33). As previously reported, the Mg^{2+} sensitivity of the open probability was substantially reduced (Fig. 2*C*). Increasing [Mg^{2+}] from 0 to 10 mM only shifted the G–V curve by ∼10 mV compared with ∼50 mV for the nonmutated BK667CY channels. Nonetheless, the conformational changes of the gating ring monitored by FRET remained unaltered by the D99A mutation (Fig. 2*D*). These results suggest that changes in FRET signals might originate from Mg^{2+} interacting with the gating ring at the high-affinity binding site in the RCK1 domain and/or the Ca^{2+} bowl located in the RCK2 domain. To explore these possibilities, we first introduced mutations D362A and D367A, which are known to alter Ca^{2+} binding to the RCK1 site (4, 31). Because in our previous work we used another mutation for this purpose (M513I), we first verified that in our construct the D362A/D367A

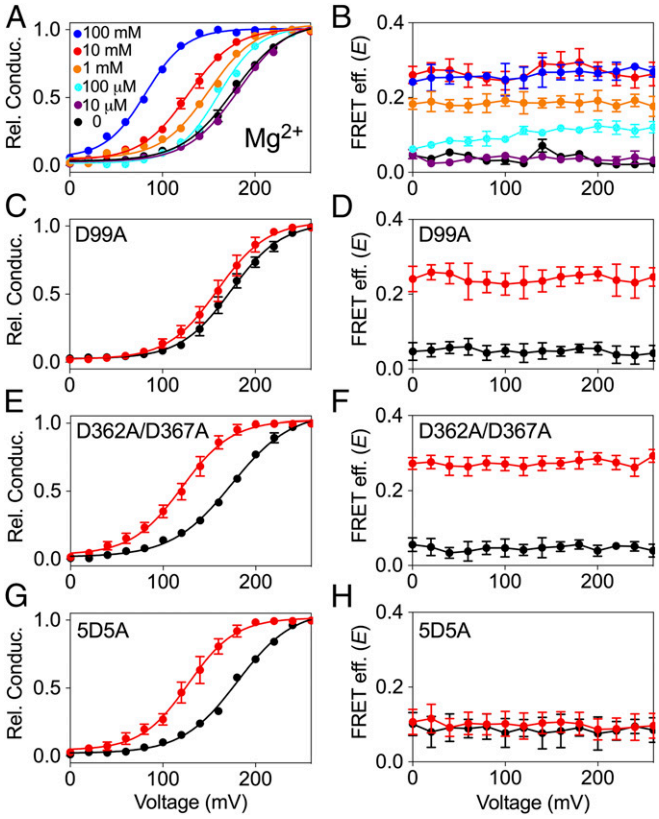

Fig. 2. Mg^{2+}-dependent movement of the BK667CY gating ring. (*A* and *B*) G–V curves and FRET efficiencies (*E*) obtained simultaneously at several Mg^{2+} concentrations. (*C* and *D*) G–V curves and *E* after mutation of the canonical Mg^{2+} binding site at the RCK1 domain. The shift in the G–V curves is prevented but the change in *E* remains the same. (*E* and *F*) G–V curves and *E* after mutation of the Ca^{2+} binding site located in RCK1 (D362A/D367A). No change in the effect of Mg^{2+} on the G–V curves nor the *E* is observed. (*G* and *H*) G–V curves and *E* after mutation of the Ca^{2+} bowl (5D5A), which abolishes the change in *E* induced by Mg^{2+} without altering the G–V curves. Data corresponding to each Mg^{2+} concentration are color coded. The solid curves in the G–V graphs represent Boltzmann fits. Data points and error bars represent average ± SEM (n = 3–10).

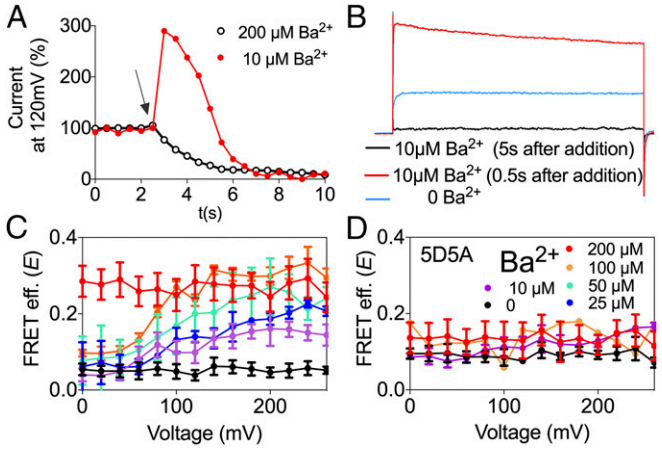

Fig. 3. Ba^{2+}-dependent movement of the BK667CY gating ring. (*A*) Time course of the normalized BK tail current before and after addition of 10 μM (red circles) and 200 μM (open black circles) Ba^{2+}. The arrow shows the moment of addition of Ba^{2+}. (*B*) Current traces recorded in the absence of Ba^{2+} (blue trace) and 0.5 s (red trace) or 5 s (black trace) after addition of 10 μM Ba^{2+}. (*C*) FRET efficiency (*E*) data obtained at several Ba^{2+} concentrations. (*D*) Change in *E* is abolished after mutation of the Ca^{2+} bowl 5D5A. Data corresponding to each Ba^{2+} concentration are color coded. Data points and error bars represent average ± SEM (n = 3–7).

mutation reduces the change in $V_{1/2}$ and *E* induced by Ca^{2+} (Fig. S2). Disruption of RCK1 Ca^{2+} binding sites did not affect the Mg^{2+}-mediated shift in voltage nor gating-ring rearrangements (Fig. 2 *E* and *F*), which remained very similar to the unaltered BK667CY constructs (Fig. 2 *A* and B). These results are consistent with the idea that there is no detectable effect of Mg^{2+} after interaction with the Ca^{2+} binding site at the RCK1 domain. We next mutated the RCK2 Ca^{2+} bowl by replacing five aspartates with five alanines, which is known to obliterate Ca^{2+} binding to this site (42). As observed previously (45), these mutations in the Ca^{2+} bowl produce a small increase in the FRET signal measured in absence of divalent ions. *E* values in the presence of 10 mM Mg^{2+} remained unaffected (Fig. 2*H*), yet the relative probability of channel opening shifted normally to the left by ∼50 mV (Fig. 2*G*). Altogether, these results strongly suggest that Mg^{2+} binding to the Ca^{2+} bowl trigger rearrangements of the gating ring. These changes in *E* are similar to those produced by Ca^{2+} binding to this site (45) (compare Fig. 2*B* with Fig. S2B) but differ on their ability to influence the open probability of the channels.

Movements of the Gating Ring Mediated by Ba^{2+}. Ba^{2+} is best known as a BK channel blocker (48). However, it has recently been reported that low concentrations of Ba^{2+} can activate BK channels by binding to the Ca^{2+} bowl (43). To monitor Ba^{2+} actions in the BK667CY constructs, we repeatedly applied voltage pulses to +120 mV from a holding potential of −70 mV and plotted the levels of K^+ currents at steady state (Fig. 3*A*). When BK667CY channels are exposed to 200 μM Ba^{2+} (Fig. 3*A*, arrow), K^+ currents are reduced as Ba^{2+} blocks the permeation pathway (Fig. 3*A*, open black circles). However, if concentrations are lowered to 10 μM, Ba^{2+} blockade is sufficiently slow to allow measurement of the activation of BK channels preceding the block (Fig. 3*A*, red circles). Fig. 3*B* shows current traces before Ba^{2+} was applied (blue trace), during the transient activation with Ba^{2+} (red trace) and after steady-state Ba^{2+} blockade was achieved (black trace). These results confirm that Ba^{2+} can also activate BK667CY channels, as reported for wild type (43). We can now assess the conformational changes of the gating ring using FRET signals irrespectively of the channels being blocked or not by Ba^{2+}. Increasing Ba^{2+} concentration from 0 to 200 μM led to an increase in the FRET signals which, as previously observed in the presence of Ca^{2+}, show voltage dependence at intermediate Ba^{2+} concentrations (Fig. 3*C*, purple, blue, cyan, and orange circles). At higher Ba^{2+} concentrations (200 μM) no voltage dependence is detected, with a maximum *E* of 0.27 ± 0.04 (n = 7) (Fig. 3*C*, red circles). These structural changes of the gating ring with Ba^{2+} follow sigmoidal relationships with K_d in the low micromolar range (Fig. S1*B*). As our previous observations with Mg^{2+}, changes in FRET signals in response to Ba^{2+} are significantly smaller than those induced by Ca^{2+} (45). This may be due to the fact that the gating-ring's rearrangements induced by Ba^{2+} binding are solely mediated by activation of the Ca^{2+}-bowl binding site. As shown in Fig. 3*D*, the 5D5A mutation abolishes the changes in *E* values, whereas mutations of the other binding sites do not modify the change in FRET signals (Fig. S3). These results indicate that Ba^{2+} binding to the Ca^{2+} bowl in RCK2 triggers a conformational change of the gating ring, which is tracked by the fluorescent proteins located in the RCK1–RCK2 linker.

Cd^{2+} Induces Conformational Changes in the Gating Ring. Even before BK channels were cloned, it was known that Cd^{2+} can activate native muscle BK channels (47). Fig. 4*A* shows that our construct BK667CY can be activated by Cd^{2+} similarly to wild-type BK channels (2). As observed with Mg^{2+} and Ba^{2+}, the magnitude of the changes in FRET signals with Cd^{2+} (0.214 ± 0.004, n = 6) is approximately half of the change in *E* obtained with Ca^{2+} (45). These gating-ring movements follow sigmoidal relationships with $[Cd^{2+}]$ with K_d in the low micromolar range (Fig. S1*C*). Independent mutations of each divalent binding site show that the activation and the conformational dynamics of the gating ring elicited by Cd^{2+} in BK667CY are mediated solely by the RCK1 binding site (Fig. 4 *C* and *D* and Fig. S4).

Independent Structural Rearrangements of RCK1 and RCK2. Given that each divalent ion species is selective for only one binding site of the gating ring, then combinations of divalent ions should provide a unique opportunity to explore the relationship between the motions of the RCK1 and RCK2 domains in a channel construct with unperturbed Ca^{2+} binding sites. Fig. 5*A* shows the effect of combining Cd^{2+} (selective for RCK1 binding site) and Ba^{2+} (selective for RCK2 binding site). In all of these patches (n = 7), *E* values were obtained from BK667CY channels that were first exposed to an intracellular solution with no divalent ions (black circles), then to

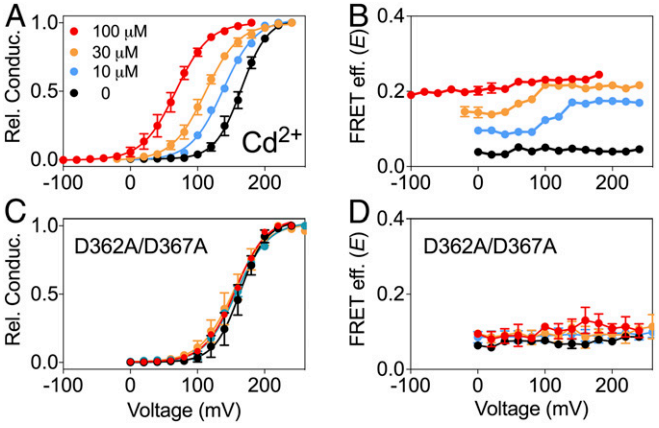

Fig. 4. Cd^{2+}-dependent movement of the BK667CY gating ring. (*A* and *B*) G–V curves and FRET efficiency (*E*) data obtained simultaneously at several Cd^{2+} concentrations. (*C* and *D*) G–V curves and *E* after mutation of the RCK1 high-affinity binding site (D363A/D367A). This mutation prevents the shift in the G–V and the change in *E*. Data corresponding to each Cd^{2+} concentration is color coded. The solid curves in the G–V graphs represent Boltzmann fits. Data points and error bars represent average ± SEM (n = 4–9).

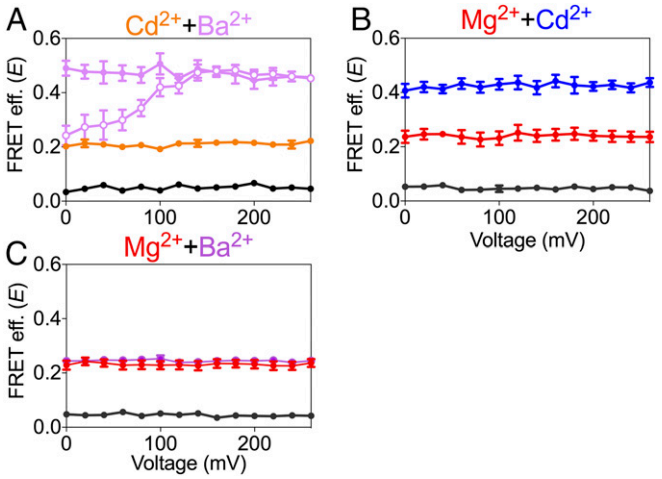

Fig. 5. Effect of combinations of divalent ions on the BK667CY gating-ring movement. (*A*) Additive effect of Cd^{2+} and Ba^{2+} on the FRET efficiency (*E*), recorded at the same patch sequentially in absence of divalent ions (black circles), with 100 μM Cd^{2+} (orange circles), with 100 μM Cd^{2+} plus 100 μM Ba^{2+} (open purple circles), and with 100 μM Cd^{2+} plus 200 μM Ba^{2+} (filled purple circles). (*B*) Additive change in *E* induced by Mg^{2+} and Cd^{2+}. *E* recorded at the same patch sequentially in absence of divalent ions (black circles), with 10 mM Mg^{2+} (red circles) and with 100 μM Cd^{2+} plus 10 mM Mg^{2+} (blue circles). (*C*) Nonadditive change in *E* of Mg^{2+} and Ba^{2+}. *E* was recorded at the same patch sequentially in absence of divalent ions (black circles), with 10 mM Mg^{2+} (red circles) and with 200 μM Ba^{2+} plus 10 mM Mg^{2+} (purple circles). Data points and error bars represent average ± SEM (n = 6–11).

100 μM Cd^{2+} (orange circles), followed by a solution containing 100 μM Cd^{2+} and 100 μM Ba^{2+} (open purple circles), and finally to a solution with 100 μM Cd^{2+} and 200 μM Ba^{2+} (filled purple circles). Remarkably, the presence of both divalent ion species at saturating concentrations produced changes in *E* comparable to those observed by using only Ca^{2+} (45). Interestingly, even the voltage dependence observed with 100 μM Ba^{2+} alone (Fig. 3*C*; orange circles) is recapitulated when Ba^{2+} and Cd^{2+} are present (Fig. 5*A*, open purple circles). Similarly, when Cd^{2+} is used with Mg^{2+} (which is selective for the RCK2 site) *E* increased additively. Fig. 5*B* shows *E* values from patches expressing BK667CY that were first exposed to 10 mM Mg^{2+} (red circles) and subsequently to 10 mM Mg^{2+} plus 100 μM Cd^{2+} (blue circles). As expected, activation of a single binding site with saturating concentrations of Ba^{2+} and Mg^{2+} (which are both selective for the Ca^{2+} bowl) rendered *E* values similar to those elicited by either Ba^{2+} or Mg^{2+} alone (Fig. 5*C*). All these results combined strongly to support the idea that the probe placed in the linker between the RCK domains tracks additive changes in FRET signals elicited independently by binding of divalent ions at their specific sites in each RCK domain.

Conformational Dynamics of BK860CY in Response to Divalent Ions. To gain further understanding of the gating-ring motions, we turned to BK860CY channels in which the FRET reporters are inserted entirely within the RCK2 domain (Fig. 1*B*). The effect of Ca^{2+} on the open probability of these channels is similar to that of wild-type BK channels (45). However, changes in *E* of this construct are qualitatively and quantitatively different from BK667CY channels. First, BK860CY channels show large values of *E* at low Ca^{2+} that decrease as [Ca^{2+}] is increased. This observation means that the fluorophores at position 860 are close at low Ca^{2+} concentration and at high concentration they move apart. Second, no voltage dependence of *E* is observed at any value of [Ca^{2+}] (45). In the presence of increasing concentrations of Mg^{2+} (Fig. 6*A*) or Ba^{2+} (Fig. 6*B*) *E* values decreased from ~0.55 to ~0.25, a significantly lower reduction than that

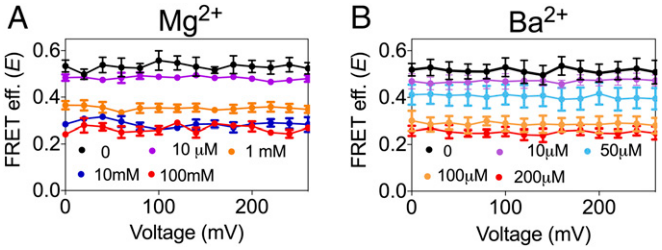

Fig. 6. BK860CY gating-ring movements by Mg^{2+} and Ba^{2+}. (*A*) FRET efficiency (*E*) obtained at different Mg^{2+} concentrations and voltages. (*B*) *E* obtained at different Ba^{2+} concentrations and voltages. In both cases, increasing the divalent concentration reduces *E*. Data corresponding to each divalent concentration are color coded. Data points and error bars represent average ± SEM (n = 5–6).

observed with Ca^{2+} (45). As previously observed with BK667CY constructs, these changes were also dependent on interactions with the Ca^{2+} bowl as assessed by the specific binding-site mutations (Figs. S5 and S6). Activation of the RCK1 binding site by Cd^{2+} in the BK860CY construct induced changes in open probability similar to those in wild-type channels and BK667CY (Fig. 7*A*). In the same way, mutating the RCK1 binding site in BK860CY abolished the allosteric effect of Cd^{2+} on the open probability (Fig. 7*C*). Strikingly, there were no changes in *E* associated with Cd^{2+} binding to BK860CY channels (Fig. 7 *B* and *D*). These results demonstrate that the conformational changes produced by Cd^{2+} interacting with the RCK1 domain that convey a shift in the open probability of the channels are not translated to the conformational changes monitored by the fluorescent protein inserted in the RCK2 domain.

Discussion

Functional measurements and site-directed mutagenesis have previously shown that Mg^{2+} and Ba^{2+} can interact preferentially with the Ca^{2+} bowl at the RCK2 domain (38, 43), whereas Cd^{2+} does it through the RCK1 domain (2). Our fluorescent protein BK channel constructs confirm these observations. We now show that these ions produce measurable conformational rearrangements of the gating ring, quantified as changes in *E*. Even though Ba^{2+} and Mg^{2+} mediate gating-ring motions in the BK667CY construct through the

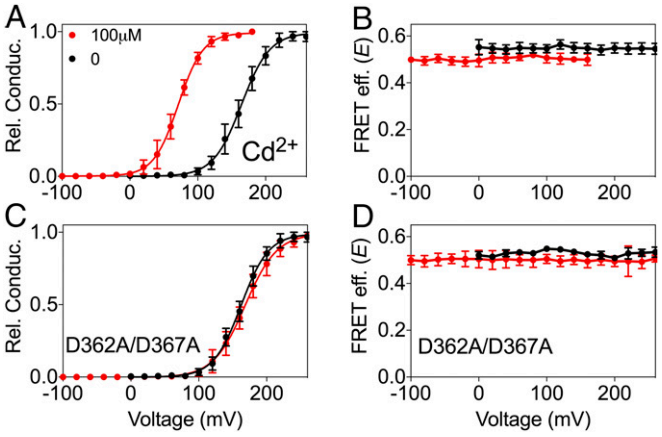

Fig. 7. The BK860CY construct does not track the gating-ring rearrangements induced by Cd^{2+}. (*A* and *B*) G–V curves and FRET efficiency (*E*) obtained simultaneously at 0 (black circles) and 100 μM Cd^{2+} (red circles). Change in Cd^{2+} concentration does not modify *E*. (*C* and *D*) G–V curves and *E* of the RCK1 high-affinity binding site mutants (D362A/D367A). The mutation prevents the shift in the G–V curves. The solid curves in the G–V graphs represent Boltzmann fits. Data points and error bars represent average ± SEM (n = 3–10).

Ca^{2+} bowl, their changes in E as well as their influence in channel activation are remarkably different. On the one hand, Ba^{2+} recapitulates a voltage-dependent component of the protein dynamics that is observed with Ca^{2+} (45), whereas Mg^{2+} does not. On the other hand, Ba^{2+} reproduces the effect of Ca^{2+} on open probability, whereas Mg^{2+} binding does not. Because our experimental approach gives information only on the changes of average distance between fluorophores, we cannot know the molecular details of such changes. Thus, a similar magnitude of FRET changes can or cannot be produced by different conformational changes. As we have discussed previously (45), we do know that the conformational changes of the gating ring reported by these fluorescent probes in response to Ca^{2+} (and now to other divalent ions) are not necessarily coupled to the open probability of the channel, and consequently they cannot be explained by the standard allosteric model (3, 37, 49, 50). Consistently, FRET signals in response to Mg^{2+} are neither related to open probability nor do they contain a voltage-dependent component. Nonetheless, occupancy of the site by Mg^{2+} could influence accessibility of Ca^{2+} and indirectly influence open probability as it has been shown previously (36). Because the ionic radius of Mg^{2+} is substantially smaller than that of Ba^{2+} or Ca^{2+} ions, it is possible that the coordinating residues from the Ca^{2+} bowl cannot form a conformation with Mg^{2+} that is compatible with activation of the channel.

In all cases tested, the maximal changes in E produced by a given divalent ion species were about half of those elicited by Ca^{2+} (45). Using the construct BK667CY, which reports protein dynamics at the RCK1–RCK2 linker, we show that the extent of the changes in E values achieved by Ca^{2+} can be obtained by combining divalent species to attain interactions with both RCK domains. These FRET changes can arise either from a change in the magnitude of the average distance between the fluorophores and/or by a change in the average time that the fluorophores reside between two unique conformation states with different FRET signals. Irrespective of the precise mechanism behind the changes of the FRET signal, our results clearly show that the magnitude of E changed additively when two species of divalent ions occupy specifically the two high-affinity binding sites.

When the fluorescent probe is confined entirely within the RCK2 domain (BK860CY construct), FRET signal changes can only be triggered by Ba^{2+} or Mg^{2+}, which are ionic species that interact with the Ca^{2+} bowl, but not by Cd^{2+}. Even though that Cd^{2+} interacts with the RCK1 domain to influence the relative probability of opening of the gate, it does not affect the RCK2 domain. All these observations suggest that the gating ring is not a rigid body and different regions of this structure can respond to divalent ions independently.

Unfortunately, we cannot relate our work to previous crystal structures of isolated gating rings (25–27). Comparison of two of these structures proposed to be in the open and closed conformations lead the authors to suggest the existence of a conformational change within the RCK1 domain with no apparent conformational change within the RCK2 domain. However, we now show that using complete BK channels, functional activation of the gating ring involves conformational changes both in the RCK1 and RCK2 domains.

In conclusion, we have demonstrated that the gating ring is a far more flexible structure than previously thought. The rearrangements triggered by divalent ion binding to the RCK1 and RCK2 domains are largely autonomous and additive. This, of course, does not exclude the possibility that both domains show functional cooperativity, particularly when Ca^{2+} ions are the ligands.

Methods

Molecular Biology and Heterologous Expression of Tagged Channels. Fluorescent BK α-subunits labeled in the position 667 or 860 with CFP or YFP were obtained using a transposon-based insertion method (51) and subcloned into the pGEMHE oocyte expression vector (52). RNA was transcribed in vitro with T7 polymerase (Ambion, Thermo Fisher Scientific), and injected at a ratio of 3:1 of CFP:YFP into *Xenopus laevis* oocytes, giving a population enriched in 3CFP:1YFP-labeled tetramers (BK667CY or BK860CY) (45). This study was performed in strict accordance with the recommendations in the *Guide for the Care and Use of Laboratory Animals* of the National Institutes of Health (53). All of the animals were handled according to approved institutional animal care and use committee (IACUC) protocols (#1253-15) of the National Institute of Neurological Disorders and Stroke. Neutralization of the Ca^{2+} bowl was achieved by mutating five consecutive aspartate residues to alanines (5D5A: 894–899) (42) on the BK667CY or BK860CY background. Elimination of RCK1 high-affinity Ca^{2+} sensitivity was achieved by double mutation D362A and D367A (2, 4). Elimination of the Mg^{2+} binding site was obtained by mutation D99A (33). Mutations were performed using standard procedures (Quikchange, Agilent Technologies).

Patch-Clamp Fluorometry and FRET. Borosilicate pipettes with a large tip (0.7–1 MΩ in symmetrical K^+) were used to obtain inside-out patches excised from *X. laevis* oocytes expressing the BK667CY or BK860CY. Currents were recorded with the Axopatch 200B amplifier and Clampex software (Axon Instruments, Molecular Devices). Recording solutions contained (in millimoles): pipette, 40 $KMeSO_3$, 100 *N*-methylglucamine–$MeSO_3$, 20 Hepes, 2 KCl, 2 $MgCl_2$, 100 μM $CaCl_2$ (pH 7.4); bath solution, 40 $KMeSO_3$, 100 *N*-methylglucamine–$MeSO_3$, 20 Hepes, 2 KCl, 1 EGTA, and $MgCl_2$ or $BaCl_2$ to give the appropriate divalent concentration previously estimated using Maxchelator software (54) (maxchelator.stanford.edu). Solutions containing different ion concentrations were exchanged using a fast solution exchange (BioLogic).

Simultaneous fluorescent and electrophysiological recordings were obtained as previously described (45). G–V curves were obtained from tail currents using standard procedures. The conformational changes of the gating ring were tracked as intersubunit changes of the FRET efficiency between the CFP and YFP as previously reported (45). The analysis of the FRET signal was performed using emission spectra ratios. We calculated the FRET efficiency as $E = (\text{ratioA} - \text{ratioA}_0)/(\text{ratioA}_1 - \text{ratioA}_0)$, where ratioA and ratioA_0 are the emission spectra ratios for the FRET signal and the control only in the presence of acceptor, respectively (44). RatioA_1 is the maximum emission ratio that we can measure in our system (45). This value of E is proportional to FRET efficiency (44). The E value shown is an average of the E values corresponding to all tetramers present in the membrane patch and represents an estimation of the distance between the fluorophores located in the same position of the four subunits of the tetramer.

ACKNOWLEDGMENTS. We thank Deepa Srikumar for technical assistance. M.H. and P.M. were supported by the intramural section of the NIH (National Institute of Neurological Disorders and Stroke). T.G. was funded by the Spanish Ministry of Economy and Competitiveness (Grant SAF2013-50085-EXP) and the European Research Council under the European Union's Horizon 2020 Research and Innovation Programme (Grant 648936).

1. Latorre R, Brauchi S (2006) Large conductance Ca^{2+}-activated K^+ (BK) channel: Activation by Ca^{2+} and voltage. *Biol Res* 39(3):385–401.
2. Zeng XH, Xia XM, Lingle CJ (2005) Divalent cation sensitivity of BK channel activation supports the existence of three distinct binding sites. *J Gen Physiol* 125(3):273–286.
3. Horrigan FT, Aldrich RW (2002) Coupling between voltage sensor activation, Ca^{2+} binding and channel opening in large conductance (BK) potassium channels. *J Gen Physiol* 120(3):267–305.
4. Xia XM, Zeng X, Lingle CJ (2002) Multiple regulatory sites in large-conductance calcium-activated potassium channels. *Nature* 418(6900):880–884.
5. Barrett JN, Magleby KL, Pallotta BS (1982) Properties of single calcium-activated potassium channels in cultured rat muscle. *J Physiol* 331:211–230.
6. Moczydlowski E, Latorre R (1983) Gating kinetics of Ca^{2+}-activated K^+ channels from rat muscle incorporated into planar lipid bilayers. Evidence for two voltage-dependent Ca^{2+} binding reactions. *J Gen Physiol* 82(4):511–542.
7. Robitaille R, Charlton MP (1992) Presynaptic calcium signals and transmitter release are modulated by calcium-activated potassium channels. *J Neurosci* 12(1):297–305.
8. Hu H, et al. (2001) Presynaptic Ca^{2+}-activated K^+ channels in glutamatergic hippocampal terminals and their role in spike repolarization and regulation of transmitter release. *J Neurosci* 21(24):9585–9597.
9. Raffaelli G, Saviane C, Mohajerani MH, Pedarzani P, Cherubini E (2004) BK potassium channels control transmitter release at CA3-CA3 synapses in the rat hippocampus. *J Physiol* 557(Pt 1):147–157.
10. Wang ZW, Saifee O, Nonet ML, Salkoff L (2001) SLO-1 potassium channels control quantal content of neurotransmitter release at the C. elegans neuromuscular junction. *Neuron* 32(5):867–881.
11. Shen KZ, et al. (1994) Tetraethylammonium block of Slowpoke calcium-activated potassium channels expressed in Xenopus oocytes: Evidence for tetrameric channel formation. *Pflugers Arch* 426(5):440–445.

12. Quirk JC, Reinhart PH (2001) Identification of a novel tetramerization domain in large conductance K(ca) channels. *Neuron* 32(1):13–23.
13. Wallner M, Meera P, Toro L (1996) Determinant for beta-subunit regulation in high-conductance voltage-activated and $Ca^{(2+)}$-sensitive K^+ channels: An additional transmembrane region at the N terminus. *Proc Natl Acad Sci USA* 93(25):14922–14927.
14. Meera P, Wallner M, Song M, Toro L (1997) Large conductance voltage- and calcium-dependent K^+ channel, a distinct member of voltage-dependent ion channels with seven N-terminal transmembrane segments (S0–S6), an extracellular N terminus, and an intracellular (S9–S10) C terminus. *Proc Natl Acad Sci USA* 94(25):14066–14071.
15. McManus OB, et al. (1995) Functional role of the beta subunit of high conductance calcium-activated potassium channels. *Neuron* 14(3):645–650.
16. Knaus HG, et al. (1994) Primary sequence and immunological characterization of beta-subunit of high conductance $Ca^{(2+)}$-activated K+ channel from smooth muscle. *J Biol Chem* 269(25):17274–17278.
17. Orio P, Rojas P, Ferreira G, Latorre R (2002) New disguises for an old channel: MaxiK channel beta-subunits. *News Physiol Sci* 17(4):156–161.
18. Contreras GF, et al. (2013) A BK (Slo1) channel journey from molecule to physiology. *Channels (Austin)* 7(6):442–458.
19. Cui J, Cox DH, Aldrich RW (1997) Intrinsic voltage dependence and Ca^{2+} regulation of mslo large conductance Ca-activated K^+ channels. *J Gen Physiol* 109(5):647–673.
20. Díaz L, et al. (1998) Role of the S4 segment in a voltage-dependent calcium-sensitive potassium (hSlo) channel. *J Biol Chem* 273(49):32430–32436.
21. Lee US, Cui J (2010) BK channel activation: structural and functional insights. *Trends Neurosci* 33(9):415–423.
22. Horrigan FT (2012) Perspectives on: Conformational coupling in ion channels: Conformational coupling in BK potassium channels. *J Gen Physiol* 140(6):625–634.
23. Ma Z, Lou XJ, Horrigan FT (2006) Role of charged residues in the S1-S4 voltage sensor of BK channels. *J Gen Physiol* 127(3):309–328.
24. Pantazis A, Olcese R (2012) Relative transmembrane segment rearrangements during BK channel activation resolved by structurally assigned fluorophore-quencher pairing. *J Gen Physiol* 140(2):207–218.
25. Wu Y, Yang Y, Ye S, Jiang Y (2010) Structure of the gating ring from the human large-conductance $Ca^{(2+)}$-gated $K^{(+)}$ channel. *Nature* 466(7304):393–397.
26. Yuan P, Leonetti MD, Pico AR, Hsiung Y, MacKinnon R (2010) Structure of the human BK channel Ca^{2+}-activation apparatus at 3.0 A resolution. *Science* 329(5988):182–186.
27. Yuan P, Leonetti MD, Hsiung Y, MacKinnon R (2011) Open structure of the Ca^{2+} gating ring in the high-conductance Ca^{2+}-activated K^+ channel. *Nature* 481(7379): 94–97.
28. Bian S, Favre I, Moczydlowski E (2001) Ca^{2+}-binding activity of a COOH-terminal fragment of the Drosophila BK channel involved in Ca^{2+}-dependent activation. *Proc Natl Acad Sci USA* 98(8):4776–4781.
29. Schreiber M, Salkoff L (1997) A novel calcium-sensing domain in the BK channel. *Biophys J* 73(3):1355–1363.
30. Schreiber M, Yuan A, Salkoff L (1999) Transplantable sites confer calcium sensitivity to BK channels. *Nat Neurosci* 2(5):416–421.
31. Zhang G, et al. (2010) Ion sensing in the RCK1 domain of BK channels. *Proc Natl Acad Sci USA* 107(43):18700–18705.
32. Yang H, et al. (2007) Mg^{2+} mediates interaction between the voltage sensor and cytosolic domain to activate BK channels. *Proc Natl Acad Sci USA* 104(46):18270–18275.
33. Yang H, et al. (2008) Activation of Slo1 BK channels by Mg^{2+} coordinated between the voltage sensor and RCK1 domains. *Nat Struct Mol Biol* 15(11):1152–1159.
34. Cox DH, Cui J, Aldrich RW (1997) Allosteric gating of a large conductance Ca-activated K^+ channel. *J Gen Physiol* 110(3):257–281.
35. Yang H, Hu L, Shi J, Cui J (2006) Tuning magnesium sensitivity of BK channels by mutations. *Biophys J* 91(8):2892–2900.
36. Shi J, Cui J (2001) Intracellular $Mg^{(2+)}$ enhances the function of BK-type $Ca^{(2+)}$-activated $K^{(+)}$ channels. *J Gen Physiol* 118(5):589–606.
37. Hu L, Yang H, Shi J, Cui J (2006) Effects of multiple metal binding sites on calcium and magnesium-dependent activation of BK channels. *J Gen Physiol* 127(1):35–49.
38. Javaherian AD, et al. (2011) Metal-driven operation of the human large-conductance voltage- and Ca^{2+}-dependent potassium channel (BK) gating ring apparatus. *J Biol Chem* 286(23):20701–20709.
39. Zhang X, Solaro CR, Lingle CJ (2001) Allosteric regulation of BK channel gating by $Ca^{(2+)}$ and $Mg^{(2+)}$ through a nonselective, low affinity divalent cation site. *J Gen Physiol* 118(5):607–636.
40. Horrigan FT, Cui J, Aldrich RW (1999) Allosteric voltage gating of potassium channels I. Mslo ionic currents in the absence of $Ca^{(2+)}$. *J Gen Physiol* 114(2):277–304.
41. Horrigan FT, Ma Z (2008) Mg^{2+} enhances voltage sensor/gate coupling in BK channels. *J Gen Physiol* 131(1):13–32.
42. Bao L, Rapin AM, Holmstrand EC, Cox DH (2002) Elimination of the BK(Ca) channel's high-affinity $Ca^{(2+)}$ sensitivity. *J Gen Physiol* 120(2):173–189.
43. Zhou Y, Zeng XH, Lingle CJ (2012) Barium ions selectively activate BK channels via the Ca^{2+}-bowl site. *Proc Natl Acad Sci USA* 109(28):11413–11418.
44. Zheng J, Zagotta WN (2003) Patch-clamp fluorometry recording of conformational rearrangements of ion channels. *Sci STKE* 2003(176):PL7.
45. Miranda P, et al. (2013) State-dependent FRET reports calcium- and voltage-dependent gating-ring motions in BK channels. *Proc Natl Acad Sci USA* 110(13):5217–5222.
46. Hu L, et al. (2003) Participation of the S4 voltage sensor in the Mg^{2+}-dependent activation of large conductance (BK) K^+ channels. *Proc Natl Acad Sci USA* 100(18): 10488–10493.
47. Oberhauser A, Alvarez O, Latorre R (1988) Activation by divalent cations of a Ca^{2+}-activated K+ channel from skeletal muscle membrane. *J Gen Physiol* 92(1):67–86.
48. Neyton J, Miller C (1988) Discrete Ba^{2+} block as a probe of ion occupancy and pore structure in the high-conductance Ca^{2+}-activated K+ channel. *J Gen Physiol* 92(5): 569–586.
49. Sweet TB, Cox DH (2008) Measurements of the BKCa channel's high-affinity Ca^{2+} binding constants: Effects of membrane voltage. *J Gen Physiol* 132(5):491–505.
50. Qian X, Niu X, Magleby KL (2006) Intra- and intersubunit cooperativity in activation of BK channels by Ca^{2+}. *J Gen Physiol* 128(4):389–404.
51. Giraldez T, Hughes TE, Sigworth FJ (2005) Generation of functional fluorescent BK channels by random insertion of GFP variants. *J Gen Physiol* 126(5):429–438.
52. Liman ER, Tytgat J, Hess P (1992) Subunit stoichiometry of a mammalian K^+ channel determined by construction of multimeric cDNAs. *Neuron* 9(5):861–871.
53. National Research Council (2011) *Guide for the Care and Use of Laboratory Animals* (National Academies Press, Washington, DC), 8th Ed.
54. Bers DM, Patton CW, Nuccitelli R (1994) A practical guide to the preparation of Ca^{2+} buffers. *Methods Cell Biol* 40:3–29.